A Computational Framework for Personalized Blood Flow Analysis in the Human Left Atrium

Tomohiro Otani,[1,3] Abdullah Al-Issa,[1] Amir Pourmorteza,[2,4] Elliot R. McVeigh,[2,5] Shigeo Wada,[3] and Hiroshi Ashikaga[1,2]

[1]Cardiac Arrhythmia Service, Division of Cardiology, Johns Hopkins University School of Medicine, 600 N. Wolfe Street, Carnegie 568, Baltimore, MD 21287, USA; [2]Department of Biomedical Engineering, Johns Hopkins University School of Medicine, Baltimore, MD, USA; [3]Department of Mechanical Science and Bioengineering, Osaka University Graduate School of Engineering Science, Osaka, Japan; [4]Department of Radiology and Imaging Sciences, National Institutes of Health Clinical Center, Bethesda, MD 20814, USA; and [5]Departments of Bioengineering, Medicine, Radiology, University of California, San Diego, La Jolla, CA, USA

Abstract—Atrial fibrillation (AF), the most common human arrhythmia, is a marker of an increased risk of embolic stroke. However, recent studies suggest that AF may not be mechanistically responsible for the stroke events. An alternative explanation for the mechanism of intracardiac thrombosis and stroke in patients with AF is structural remodeling of the left atrium (LA). Nevertheless, a mechanistic link between LA structural remodeling and intracardiac thrombosis is unclear, because there is no clinically feasible methodology to evaluate the complex relationship between these two phenomena in individual patients. Computational fluid dynamics (CFD) is a powerful tool that could potentially link LA structural remodeling and intracardiac thrombosis in individual patients by evaluating the patient-specific LA blood flow characteristics. However, the lack of knowledge of the material and mechanical properties of the heart wall in specific patients makes it challenging to solve the complexity of fluid–structure interaction. In this study, our aim was to develop a clinically feasible methodology to perform personalized blood flow analysis within the heart. We propose an alternative computational approach to perform personalized blood flow analysis by providing the three-dimensional LA endocardial surface motion estimated from patient-specific cardiac CT images. In two patients (case 1 and 2), a four-dimensional displacement vector field was estimated using nonrigid registration. The LA blood outflow across the mitral valve (MV) was calculated from the LV volume, and the flow field within the LA was derived from the incompressible Navier–Stokes equation. The CFD results successfully captured characteristic features of LA blood flow observed clinically by transesophageal echocardiogram. The LA global flow characteristics and vortex structures also agreed well with previous reports. The time course of LAA emptying was similar in both cases, despite the substantial difference in the LA structure and function. We conclude that our CT-based, personalized LA blood flow analysis is a clinically feasible methodology that can be used to improve our understanding of the mechanism of intracardiac thrombosis and stroke in individual patients with LA structural remodeling.

Keywords—Image-based simulation, Computed tomography, Computational fluid dynamics, Cardiac mechanics, Left atrium.

ABBREVIATIONS

AF	Atrial fibrillation
CFD	Computational fluid dynamics
CT	Computed tomography
LA	Left atrium
LAA	Left atrial appendage
LV	Left ventricle
MV	Mitral valve
PV	Pulmonary vein
TEE	Transesophageal echocardiogram
3D	Three-dimensional
4D	Four-dimensional

Address correspondence to Hiroshi Ashikaga, Cardiac Arrhythmia Service, Division of Cardiology, Johns Hopkins University School of Medicine, 600 N. Wolfe Street, Carnegie 568, Baltimore, MD 21287, USA. Electronic mail: hashika1@jhmi.edu

INTRODUCTION

Atrial fibrillation (AF) is associated with an increased risk of embolic stroke.[32] However, recent studies using extended electrocardiographic monitor-

ing revealed that most patients with acute stroke had no evidence of AF within 1 month prior to the event.[5,8] In addition, even a single 6-min episode of atrial arrhythmia is associated with a greater than two-fold risk of ischemic stroke.[13] These findings strongly suggest that AF may be a marker of an elevated thromboembolic risk, but may not be mechanistically responsible for the events.[24] Instead, alterations in cardiac structure and function that serve as an arrhythmic substrate for AF may be causally related to thromboembolism. In fact, indices of left atrial (LA) structural remodeling, including larger LA size,[3,10,18,30] larger extent of LA fibrosis,[7] lower LA function,[14,26,33] and lower LA appendage (LAA) function[2,23] are known markers of stroke. Nevertheless, a mechanistic link between LA structural remodeling and intracardiac thrombosis is unclear, because there is no clinically feasible methodology to evaluate the complex relationship between these two phenomena in individual patients.

Computational fluid dynamics (CFD) is a powerful tool that can provide a methodology to link LA structural remodeling and intracardiac thrombosis in individual patients by evaluating the patient-specific LA blood flow characteristics.[19,34] However, one of the challenges of personalized CFD analysis within the heart is the complexity of fluid–structure interaction between the blood flow and the heart wall, mainly resulting from the lack of knowledge of the material and mechanical properties of the heart wall in specific patients. In this study, our aim was to develop a clinically feasible methodology to perform personalized blood flow analysis within the heart. We propose an alternative approach to perform personalized blood flow analysis by providing the three-dimensional (3D) LA endocardial surface motion estimated from patient-specific cardiac CT images. In essence, our approach reduces the cardiac CFD analysis to a moving boundary problem, which is clinically tractable in individual patients. The effectiveness of our approach is demonstrated by numerical examples of two human patients.

MATERIALS AND METHODS

The workflow of the LA personalized blood flow analysis is shown in Fig. 1. The protocol was approved by the Institutional Review Board of the Johns Hopkins Medicine.

Patient-Specific Cardiac Structure

In this study we used cardiac CT images of two patients with a history of AF (case 1 and case 2) but
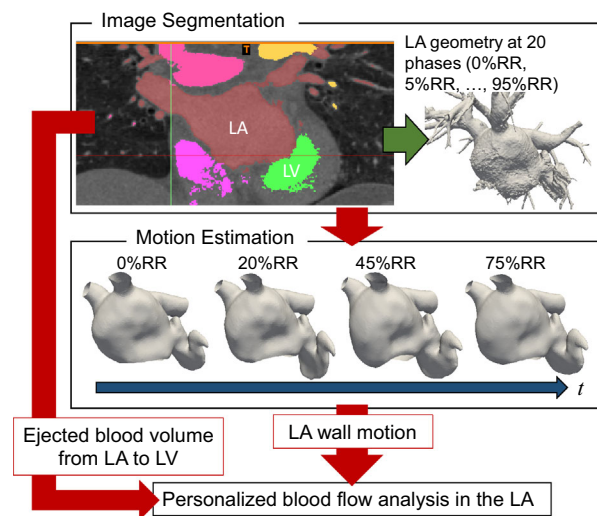

FIGURE 1. Workflow of personalized blood flow analysis in the left atrium. *Image Segmentation.* The CT images were segmented to reconstruct the left atrial (LA) surface structure and measure the left ventricular (LV) volume for a total of 20 phases in a cardiac cycle (0%RR, 5%RR, …, 95%RR), where the RR indicates the cycle length. *Motion Estimation.* The LA wall motion was estimated by a nonrigid registration method.[25] Personalized blood flow analysis in the LA was performed with patient-specific LA wall motion and ejected blood volume from LA to LV calculated by the LV volume change.

without a prior history of stroke or transient ischemic attack. We acquired the CT images during normal sinus rhythm prior to catheter ablation of AF using a 64-slice multi-detector CT scanner (Aquilion 64, Toshiba America Medical Systems, Inc. Tustin, CA). We reconstructed the volumetric CT images for a total of 20 phases (0%RR, 5%RR, … , 95%RR) during the cardiac cycle. Here, the RR indicates the cycle length, or the interval between two consecutive electrocardiographic R waves, and 0%RR indicates electrocardiographic ventricular end-diastole. The reconstructed image matrix size was $512 \times 512 \times 298$ for case 1 and $512 \times 512 \times 352$ for case 2. The in-plane pixel size was 0.5×0.5 mm^2, the through-plane slice thickness was 1.0 mm, and slice gap was 0.5 mm, resulting in a 3D image matrix of $0.5 \times 0.5 \times 0.5$ mm^3. We segmented the endocardial surface of the LA and the left ventricle (LV) at all the phases on the basis of signal intensity using the cardiovascular segmentation tool of Mimics Medical 18.0 (Materialise, Inc. Plymouth, MI). We removed the pulmonary veins (PVs) beyond the first bifurcation using MeshMixer (Version 1.09.293; Autodesk, Inc. San Rafael, CA). We defined the triangular LA endocardial surface geometry at the reference phase (0%RR) as the template mesh using Pointwise (Version V17.3R1; Pointwise, Inc. Fort Worth, TX) with the base element size of 1.5 mm. This base element size was determined from the spatial resolution of

the CT image (slice thickness of 1 mm) and a measurement error of one in-plane pixel size (=0.5 mm). The LA structure of both the cases is shown in Fig. 2. Of note, case 1 also underwent transesophageal echocardiogram (TEE) with Doppler-based blood velocity measurements within the LA under general anesthesia at a separate time point. The blood velocity data from TEE was used to validate our CFD results.

Patient-Specific Cardiac Function

We used a nonrigid registration method developed by Pourmorteza *et al.*[25] to estimate the cardiac motion, which directly computes the 3D displacement fields between the target mesh in the reference phase and a target mesh in all the other (deformed) phases such that every triangle on the template mesh has a corresponding triangle on each of the target mesh. To obtain the four-dimensional (4D) continuous displacement field $\mathbf{u}(t)$ of the endocardial LA surface, we interpolated the discrete displacement fields $\bar{\mathbf{u}}_i$ given in 20 phases ($i = 1, 2, \ldots, 20$) using inverse Fourier series expansion.[6]

$$\mathbf{u}(t) = \sum_{k=0}^{L} \mathbf{F}_k \exp\left(\frac{2\pi ikt}{T}\right), \tag{1}$$

where T is the cycle length, L is the maximum Fourier mode, and $\mathbf{F}_k$ is the Fourier coefficient, obtained from the Fourier transform of $\bar{\mathbf{u}}_i$, which is the magnitude at frequency k/T. Since our CT system required approximately 0.15 s to reconstruct the cardiac images in each phase using the half-scan reconstruction method,[21] we

removed $\mathbf{F}_k$ in the high frequency domain ($>1/0.15 \approx 6.7$ s^{-1}) which likely contained measurement errors.

Patient-Specific Left Atrial Blood Flow Analysis

For the blood flow analysis, we created tetrahedral volumetric meshes in the LA at the reference phase using Pointwise. With the base element size of 1.5 mm, the total number of volumetric elements was 366,909 and 549,299 in case 1 and 2, respectively. We conducted a mesh convergence study to confirm that the volumetric element size did not substantially influence the solutions (see Appendix S1, *Electronic Supplementary Material*). We performed the LA blood flow analysis using OpenFOAM 2.3.1 (http://www.openfoam.com/). We assumed the blood to be an incompressible Newtonian fluid with density ρ of 1.05×10^3 kg/m^3 and viscosity μ of 3.5×10^{-3} Pa s, because the non-Newtonian effects on the global blood flow characteristics in large domains such as the LA are considered to be negligible.[20] The flow in the LA was modeled with the incompressible Navier–Stokes equation and the continuity equation, given by

$$\frac{\partial \mathbf{v}}{\partial t} + \mathbf{v} \cdot \nabla \mathbf{v} = -\frac{1}{\rho}\nabla p + \frac{\mu}{\rho}\nabla^2 \mathbf{v}, \tag{2}$$

$$\nabla \cdot \mathbf{v} = 0, \tag{3}$$

where $\mathbf{v}$ is the velocity vector and p is the pressure (see Appendix S2, *Electronic Supplementary Material*). We treated the flow as laminar because the mean Reynolds number through the mitral valve (MV) during diastole was approximately 2400 and 1100 in case 1 and case 2, respectively. The blood flow across the MV was calculated from the changes in the LV volume during ventricular diastole measured from CT images. To minimize the computational cost and the impact of boundary conditions on the CFD analysis, we modeled the LV and each of the distal PV beyond the first bifurcation as a cylinder. We also interpolated the 4D displacement fields smoothly in the PVs and the LV surfaces to avoid generating defect volume elements with high aspect ratio or non-orthogonality (see Appendix S3, *Electronic Supplementary Material*). We calculated the 4D displacement field of the LV surface to allow the LV volume change measured from the CT images. We considered the MV to be closed during ventricular systole, open during ventricular diastole, and the time required for MV opening and closing to be negligible. We defined ventricular systole and diastole by the time course of the LV volume (Fig. 3, top row). We created two sets of volume mesh to calculate the blood flow depending on the MV configuration.
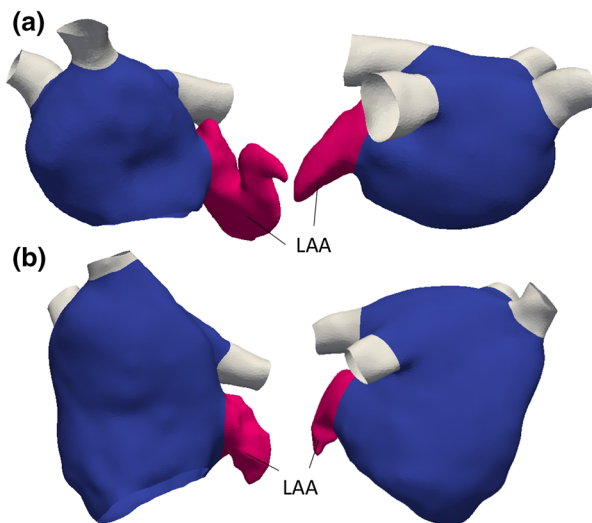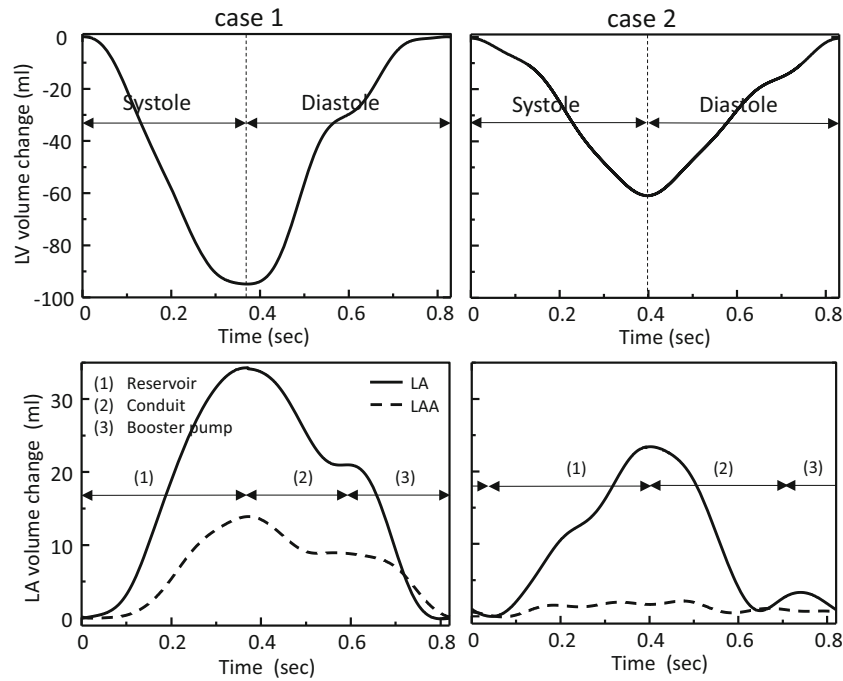

FIGURE 2. Patient-specific left atrial structure. The structure of the left atrium (LA, blue) and the left atrial appendage (LAA, red) represents 0%RR in both case 1 (a, top row) and case 2 (b, bottom row). Anterior view (left column); posterior view (right column).

FIGURE 3. Time course of left ventricular volume change (top row) and volume changes of left atrium (LA, solid line) and left atrial appendage (LAA, dashed line) (bottom row) during the cardiac cycle. The left column show case 1 and the right column show case 2. Arrows in the top row indicate the duration of systole and diastole; arrows in the bottom row indicate the duration of each phase of LA function (reservoir, conduit and booster pump).

When the MV was open, the volume mesh included the LA and the LV. When the MV was closed, the volume mesh included only the LA. The LA flow fields in transition between systole and diastole were interpolated using data mapping function in the OpenFOAM ("mapFields"). The initial velocity magnitude in the LV at the beginning of ventricular diastole was set to zero.

Computation

The boundary conditions for the CFD studies were as follows. We determined the velocity vectors from time t to $t + \Delta t$ in each time step at the surface boundary from the surface displacement fields in Eq. (1). We employed the zero-gradient pressure condition at the distal end of each PV, where we determined the velocity by the flow direction: zero-gradient velocity for the PV inflow and a fixed velocity calculated from the flux through the boundary for the PV outflow. This boundary condition was chosen to reproduce both inflow and outflow of the PVs that are observed during the cardiac cycle in human heart.[29] The pressure p is determined such that the total pressure $[p + \frac{1}{2}\rho(\mathbf{v} \cdot \mathbf{v})]$ is equal to zero. The MV annulus during ventricular systole was treated as a surface boundary. We conducted the blood flow analysis in each case with the time increment of 1×10^{-4} s. We

defined convergence in each time step by the tolerance of velocity and pressure lower than 1×10^{-5} and 1×10^{-8}, respectively. We computed a total of five cardiac cycles in each case.

Vortex Structures Within the LA

The 3D vortex structure using q_2 criterion is often used to assess the cardiac flow characteristics.[6,28,31] It is calculated as the second invariant of the velocity gradient tensor q_2, given by

$$q_2 = \frac{1}{2}(\Omega_{ij}\Omega_{ij} - S_{ij}S_{ij}) \qquad (4)$$

where Ω_{ij} and S_{ij} are the rotation and shear strain tensor, respectively. We used this criterion to visualize the vortex structures as the iso-surface of q_2 in the flow field.

Left Atrial Appendage Flow Characteristics

We assessed the LAA flow characteristics by two indices. First, flow dissipation within the LAA was assessed by the flow kinetic energy in the LAA, defined by

$$\text{Kinetic energy} = \int_{V_{\text{LAA}}} \frac{1}{2}\rho(\mathbf{v} \cdot \mathbf{v})dV \qquad (5)$$

where V_{LAA} is the LAA volume. Second, blood stasis within the LAA was assessed by solving the transportation of the passive scalar ϕ in the flow field within the LAA. The passive-scalar transport analysis is one of the efficient and cost-effective techniques to visualize the blood flow characteristics[16,27] and to quantify blood flow stasis.[12,22] ϕ is expressed as the convection–diffusion equation, given by

$$\frac{\partial \phi}{\partial t} + \mathbf{v} \cdot (\nabla \phi) - D\nabla^2 \phi = 0 \qquad (6)$$

where D is the diffusion coefficient of $1 \times 10^{-9}\,\mathrm{m^2/s}$[16,28] (see Appendix S4, *Electronic Supplementary Material*). At the beginning of the third cardiac cycle, ϕ was set to zero in the entire calculation domain except within the LAA where ϕ was set to one. To quantify blood stasis within the LAA, the residual fraction of ϕ was calculated as

$$\text{Residual fraction} = \frac{1}{V_{LAA}^0} \int_{V_{LAA}} \phi\, dV \qquad (7)$$

where V_{LAA}^0 is the LAA volume at the initial condition.

RESULTS

Baseline Characteristics

The baseline characteristics of each patient are shown in Table 1. The cycle length was 0.82 s in both cases, equivalent to the heart rate of approximately 73 beats per minute. The LA volume in case 2 was approximately 2.3 times larger than that of case 1, whereas the LAA volume of case 2 was smaller than the case 1.

Time Course of Left Atrial and Left Atrial Appendage Volume

The time course of LA and LAA volume with reference to the ventricular end-diastole was calculated in both cases from motion estimation results (Fig. 3, bottom row). The time course clearly showed three

characteristic phases of LA function in both cases: (1) Reservoir phase: pulmonary venous return during the LV systole, (2) Conduit phase: pulmonary venous return during the LV early diastole, and (3) Booster pump phase: augmentation of the LV filling during the LV late diastole. In case 1, the LA volume rapidly increased and reached its peak (volume increase ~35 mL) at the end of the reservoir phase. The LA volume fell to a plateau at the end of the conduit phase, and further decreased to return the baseline at the end of the booster pump phase. The LAA volume showed a similar trend, reaching its peak (volume increase ~15 mL) at the end of the reservoir phase. Together, the LA and the LAA accounted for approximately 60% of the LV filling volume, which is consistent with our previous data in patients using cardiac MRI.[14] In case 2, the LA volume increased during the reservoir phase and reached its peak with a volume increase of ~20 mL. Unlike case 1, the LA volume then rapidly fell to close to the baseline during the conduit phase, and the booster pump phase had only a small volume increase (< 5 mL). Furthermore, the reservoir and the conduit phases were longer, whereas the booster pump phase was shorter than those of case 1. The LAA volume change was consistently small during the entire cardiac phase (< 5 mL).

Comparison Between CFD and Measurement Results

The flow features at the LA-LAA junction (LAA os) was compared between the CFD results and clinical measurement using pulsed-Doppler TEE in case 1(red arrow in Fig. 4(a)). Figure 4(b) shows the velocity magnitude measured over the cardiac cycle, which successfully captured four characteristic features of blood flow in this location[1]: (1) *LAA filling*: negative velocity with high magnitude; (2) *Systolic reflection waves* variable numbers of alternating positive and negative velocities with diminishing magnitudes; (3) *Early diastolic LAA flow* positive velocity with low magnitude; and (4) *LAA contraction* positive velocity with high magnitude. In this specific patient, the early diastolic LAA flow included both positive and negative velocities (Fig. 4(b)), which likely represents a complex interaction between passive LAA emptying during rapid LV filling and continuous LAA filling from PV inflow.[1] To compare the CFD results against the TEE measurements, the corresponding sampling point and pulse direction were identified in the mesh (Fig. 4(c)). Figure 4(d) shows the velocity magnitude over time from the CFD results, which successfully captured the four characteristic features of blood flow with magnitudes similar to that of TEE measurements (arrows 1–4).

TABLE 1. Baseline characteristics.

	Case 1	Case 2
Cycle length (s)	0.82	0.82
LA volume (0%RR) (mL)	96.8	227.3
LAA volume (0%RR) (mL)	13.9	8.47
LV volume (0%RR) (mL)	135	160

LA, left atrium; LV, left ventricle; LAA, left atrial appendage; RR, electrocardiographic R–R interval.
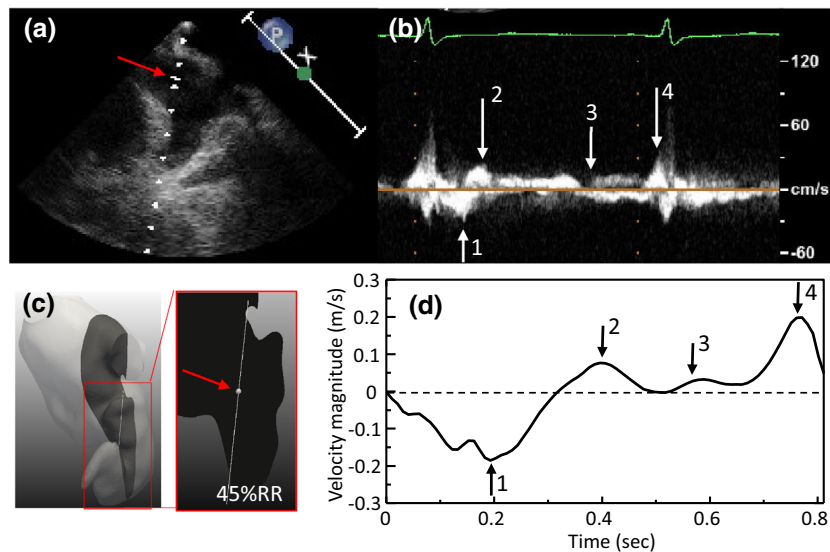
FIGURE 4. Validation against flow velocity measurements by transesophageal echocardiogram (TEE). (a) TEE images of the left atrial appendage (LAA) (90° angle). The red arrow shows the sampling point of the velocity magnitude measurements along the dashed line from bottom to top of the image. (b) Time course of flow velocity magnitude by pulsed-Doppler TEE tracing. (c) Corresponding sampling point and direction along which to measure the flow velocity magnitude in the CFD results. (d) Time course of flow velocity magnitude from the CFD results. The arrows 1 through 4 indicate characteristic features of LAA blood flow (see text for details).

Left Atrial Global Flow Characteristics

For the five cardiac cycles calculated in each case, flow characteristics reached a stable condition and became periodic within the first three cardiac phases. Therefore, we did not include the first two cardiac cycles but included only the last three cardiac cycles in the final analysis.

Figure 5 shows the streamlines of blood flow in a representative cardiac cycle in the posterior view of the LA. In case 1, the blood flow from both the left PVs swirled clockwise along the top of the LA and the septum during the reservoir phase (Fig. 5 (case 1, 26%RR)). During the conduit phase, this swirling flow was replaced by longitudinal flow of high velocity magnitude coming from all PVs to pass through the MV (Fig. 5 (case 1, 57%RR)). At the end of the conduit phase, the longitudinal flow was replaced transiently by the swirling flow (Fig. 5 (case 1, 73%RR)). During the booster pump phase the swirling flow immediately disappeared, followed by appearance of the flow coming into all PVs (Fig. 5 (case 1, 90%RR)). Case 2 also generated the clockwise swirling flow in the posterior view (Fig. 5 (case 2, 20%RR)), which persisted throughout the cardiac cycle (Fig. 5 (case 2, 53%RR); Fig. 5 (case 2, 75%RR); and Fig. 5 (case 2, 90%RR)). The velocity magnitudes were consistently small compared with those of case 1.

The 3D vortex structures visualized by the iso-surface of q_2 are shown in Fig. 6. In case 1, the vortex rings were generated at the superior segment of the LA due to the flow coming out of each PV (Fig. 6 (case 1, 45%RR); Fig. 6 (case 1, 58%RR)). The vortex rings became larger during the conduit phase (Fig. 6 (case 1, 77%RR)) and expanded in the whole LA (Fig. 6 (case 1; 99%RR)). In contrast, in case 2 the vortex rings remained small consistently throughout the cardiac cycle.

Left Atrial Appendage Flow Characteristics

Figure 7 shows the time course of kinetic energy within the LAA in both cases. In case 1, kinetic energy was 0.3×10^{-4} J at baseline, which reached the maximum at 1.7×10^{-4} J during the mid-reservoir phase. It then decreased to 0.5×10^{-4} J at the end of the reservoir phase but increased again to 1.1×10^{-4} J until the mid-conduit phase. Kinetic energy then decreased again to 0.3×10^{-4} J and remained low until the end of the conduit phase. It rapidly increased to 1.5×10^{-4} J at the beginning of the booster pump phase and rapidly decreased to the baseline at 0.3×10^{-4} J. In case 2, kinetic energy was approximately one order of magnitude smaller than that of case 1. As in case 1, kinetic energy slightly increased during the reservoir and the conduit phases. However,
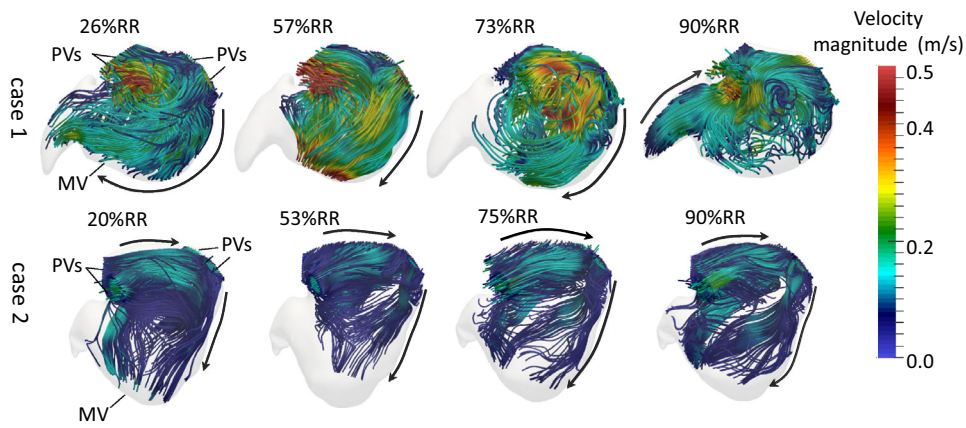
FIGURE 5. Streamlines of blood flow during a representative cardiac cycle in the posterior view. Top row shows case 1; Bottom row shows case 2.
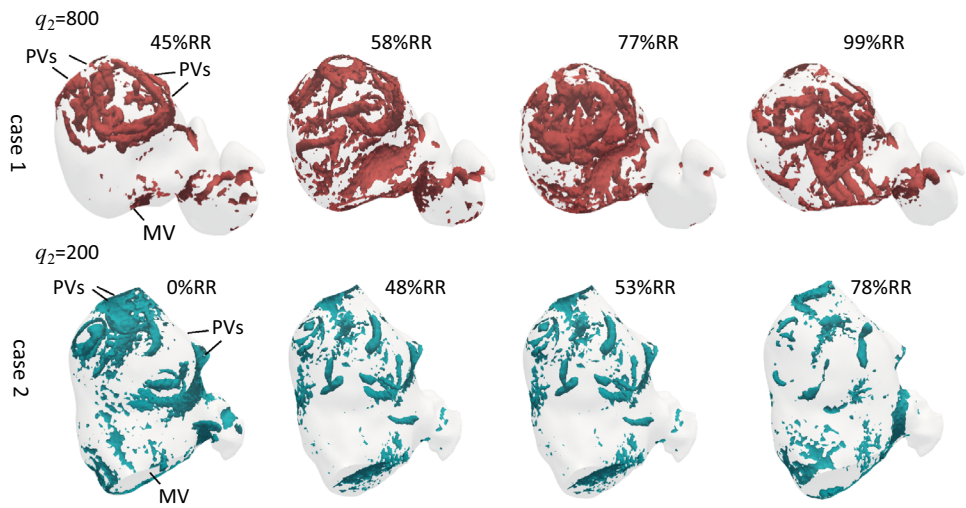

FIGURE 6. Vortex structures during a representative cardiac cycle in the anterior view. Top row shows case 1 ($q_2 = 800$); Bottom row shows case 2 ($q_2 = 200$). See the main text for details.
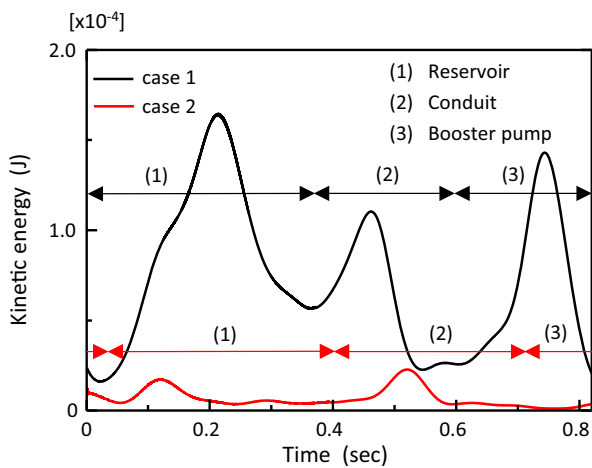

FIGURE 7. Time course of left atrial appendage kinetic energy. The black line indicates case 1 and the red line indicates case 2. Black and red arrows indicate each phase of LA function (reservoir, conduit and booster pump) in the respective cases.

unlike case 1, there was no increase in kinetic energy during the booster pump phase. In addition, although the booster pump phase was shorter than that of case 1, kinetic energy did not go back to the baseline until ~50 ms into the next cardiac cycle due to a delay in each phase compared with case 1.

Figure 8(a) shows the iso-surface of a passive scalar $\phi = 0.8$ at ventricular end-diastole for the last three cardiac cycles (Beat 1–3). The results indicate that it took both cases three full cardiac cycles to empty the bulk of blood out of the LAA, although some amount of blood still remained at the periphery of the LAA at the end of Beat 3 (Fig. 8A (d)). The time course of residual fraction is shown in Fig. 8B. The residual fraction in both cases decreased with oscillation mainly due to systolic reflection waves with alternating positive and negative velocities during the reservoir phase. In both cases the residual fraction approached to zero at the end of beat 3, which is consistent with Fig. 8A.
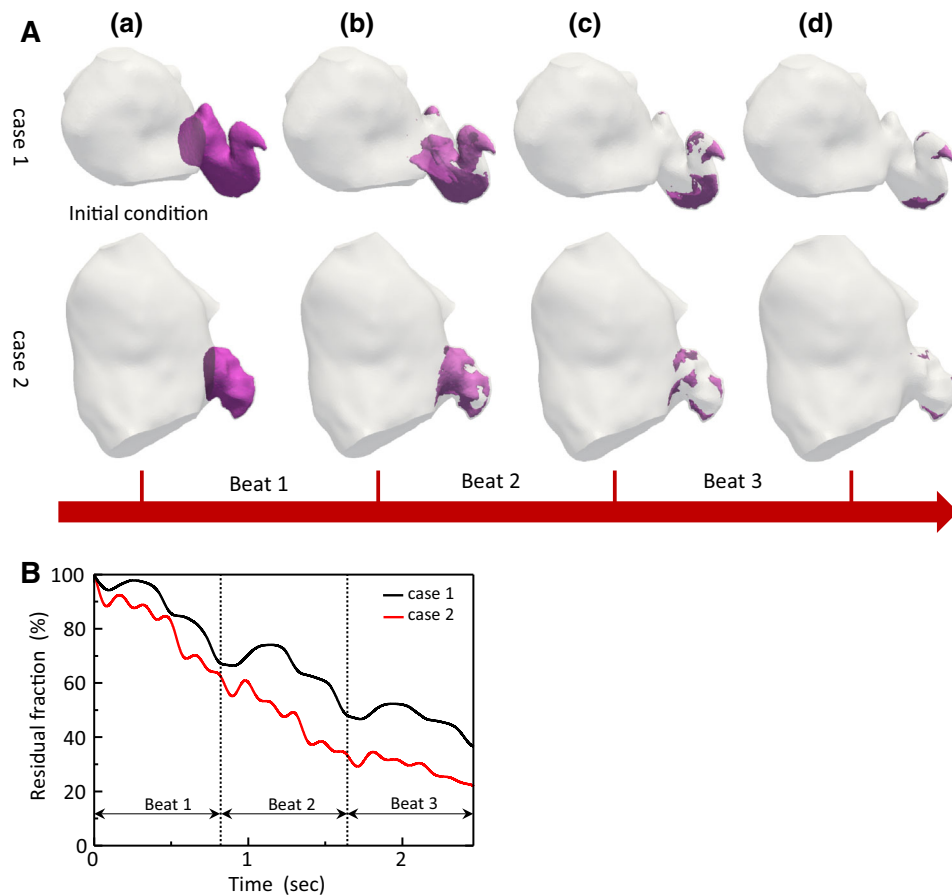
FIGURE 8. Left atrial appendage (LAA) blood emptying during the last three cardiac cycles (beat 1–3). A: Iso-surface of passive scalar $\phi = 0.8$ at the end of each heart beat except the initial condition (left column, $\phi = 1$). Top row shows case 1; Bottom row shows case 2. Both cases are in the anterior view. B: Time course of left atrial appendage (LAA) residual fraction during the last three cardiac cycles (beat 1–3). The black line indicates case 1 and the red line indicates case 2.

DISCUSSION

In this study, we performed a personalized LA blood flow analysis in two cases based on the patient-specific LA structure, endocardial surface motion and blood outflow into the LV. The time course of the LA volume clearly showed the three characteristic phases of the LA function in both cases (Fig. 3, bottom row), which is consistent with measurement results in our previous work using cardiac MRI.[14] However, the duration of each phase and the magnitude of volume change were substantially different between the two cases. These differences between the two cases are likely related to patient-specific LA structure and function. For example, the LA volume of case 2 was 2.3 times larger than that of case 1 (Table 1), and this abnormal structure may account for the longer reservoir and conduit phases and smaller magnitudes of volume changes in case 2 compared with those of case 1. These differences underscore the strength of our personalized approach, which provides clinically relevant patient-specific data.

The time course of the LA global blood flow in case 1 successfully recapitulates the blood flow characteristics of the healthy human LA,[11] including (1) *Reservoir phase* appearance of a swirling flow mainly from the left PVs in the LA; (2) *Early conduit phase* disappearance of the swirling flow; (3) *End of conduit phase* reappearance of the swirling flow; and (4) *booster pump phase* disappearance of the swirling flow and appearance of the flow coming into all the PVs (Fig. 5(top row)). Our CFD framework also successfully reproduced the characteristic features of blood flow at the LAA os. Therefore, we believe that our computational framework for the personalized blood flow analysis is robust and can be used clinically to evaluate the global features of the LA blood flow field in individual patients.

It is important to note that the cardiac CT protocol from which motion estimation for the personalized blood flow analysis is performed is clinically practical. With a current state-of-the-art 320-slice multidetector CT scanner, the contrast-to-noise ratio sufficient for the motion estimation can be obtained with a radiation

dose of < 0.8 mSv using a low-dose cardiac functional CT protocol with retrospective ECG gating. This radiation dose is equivalent to that of less than two mammograms.[2]

The LAA is the most common site of intracardiac thrombus,[4] therefore evaluation of blood flow characteristics within the LAA is clinically important for assessment of cardioembolic stroke risk. We chose to use flow kinetic energy to quantify the strength of and evaluate the characteristics of blood flow within the LAA because it is a straightforward scalar parameter that is physically meaningful. We found that kinetic energy of the LAA was consistently high during the reservoir phase in case 1, whereas kinetic energy during the same phase in case 2 was substantially smaller (Fig. 7). These findings suggest that the high kinetic energy during the reservoir phase was caused by the LAA filling as the LA swirling flow entered the LAA (Fig. 5 (case 1, 26%RR)). Since depressed LA reservoir function during normal sinus rhythm is associated with stroke,[14] it is possible that the high kinetic energy during the reservoir phase contributes to maintaining the blood flow in and out of the LAA to minimize blood stasis that could lead to thrombogenesis. However, since neither case 1 nor case 2 had a history of stroke, further study with a larger sample size is needed to confirm this speculation.

In contrast to kinetic energy, the time course of LAA emptying by passive-scalar transport analysis was similar in both cases, despite the substantial difference in the LA structure and function. In case 1, the blood almost completely flowed away from the LAA by the end of Beat 3 but a small amount remained in the periphery of the LAA, primarily because of the complex LAA morphology. In case 2, the blood steadily flowed away from the LAA by the end of Beat 3, but remained in some small peripheral regions of the LAA similar to case 1 (Fig. 8A(d)). In fact, it was unexpected to find a similar time course in these two cases with substantial difference in the degree of structural remodeling (Fig. 8B). This somewhat counterintuitive finding implies that a smaller size and a relatively simple morphology of the LAA in case 2 may promote blood emptying and compensate for the flow dissipation due to structural remodeling. These findings are also consistent with previous reports that patients with a simpler LAA morphology are less associated with stroke than those with more complex LAA morphology.[9,15,17] Since our methodology allows personalized LA blood flow analysis that incorporates a number of clinically important patient-specific factors such as the LA/LAA size, LA/LAA function, and the LAA morphology, it can be used to improve our understanding of the mechanism of intracardiac thrombosis and stroke in individual patients with LA structural remodeling.

Limitations

The strength of our approach lies in the fact that it utilizes the 3D LA endocardial surface motion derived from patient-specific cardiac CT images, thus compensates for the lack of knowledge of the material and the mechanical properties of the heart wall in specific patients. Although our approach can successfully describe the global features of blood flow in the LA and the LAA, it should be noted that the motion estimation techniques using nonrigid registration in general are not physically consistent, and the accuracy highly depends on the spatiotemporal resolution and the image quality of the CT images. In addition, the base element size of motion estimation and CFD analysis is also limited by the spatial resolution of the original CT image. Since the main objective of our study was to develop a clinically feasible methodology to perform personalized blood flow analysis, we avoided deviating from the patient data by artificially creating small volume elements by interpolation. However, our mesh convergence study confirms that the base element size of 1.5 mm based on the spatial resolution of the original CT image is sufficiently fine (see Appendix S1, *Electronic Supplementary Material*). In terms of CFD analysis, it is possible that our approach with a simplified MV configuration did not accurately reproduce the true flow field around the MV. However, we successfully reproduced the global flow characteristics in the LA and the LAA described in the literature. We were not able validate the individual PV inflow because the clinical data that quantified different blood flow volume through each PV was not available. Although our CFD approach was validated against TEE, which is the clinical standard to evaluate the LAA function and blood flow, different physiological conditions at the time of CT and TEE acquisitions such as the heart rate, the ratio of the systolic over the diastole phase, volume status, preload, afterload and autonomic tone, make quantitative comparison of flow parameters between the CFD and the TEE challenging and somewhat meaningless. In addition, the velocity measurement by TEE is limited to a two-dimensional plane whose coordinate system cannot be determined. Therefore, in this study we focused on analysis of four characteristic features of the LAA blood flow that are well described and clinically meaningful. In future studies, we plan to utilize four-dimensional MRI with 3D flow mapping for more robust quantitative validation of our computational approach.

Conclusions

We developed a computational framework to perform CT-based, personalized blood flow analysis in the LA. Our methodology successfully computes the LA blood flow using the patient-specific LA structure and function obtained from the cardiac CT images. Our personalized LA blood flow analysis is a clinically feasible methodology that can be used to improve our understanding of the mechanism of intracardiac thrombosis and stroke in individual patients with LA structural remodeling.

ELECTRONIC SUPPLEMENTARY MATERIAL

The online version of this article (doi:10.1007/s10439-016-1590-x) contains supplementary material, which is available to authorized users.

CONFLICT OF INTEREST

None.

REFERENCES

[1]Agmon, Y., B. K. Khandheria, F. Gentile, and J. B. Seward. Echocardiographic assessment of the left atrial appendage. *J. Am. Coll. Cardiol.* 34:1867–1877, 1999. doi:10.1016/S0735-1097(99)00472-6.

[2]Al-Issa, A., Y. Inoue, J. Cammin, Q. Tang, S. Nazarian, H. Calkins, E. K. Fishman, K. Taguchi, and H. Ashikaga. Regional function analysis of left atrial appendage using motion estimation CT and risk of stroke in patients with atrial fibrillation. Eur. Hear. J. Cardiovasc. Imaging jev207, 2015. doi:10.1093/ehjci/jev207.

[3]Benjamin, E. J., R. B. D'Agostino, A. J. Belanger, P. A. Wolf, and D. Levy. Left atrial size and the risk of stroke and death: the Framingham heart study. *Circulation* 92:835–841, 1995. doi:10.1161/01.CIR.92.4.835.

[4]Blackshear, J. L., and J. A. Odell. Appendage obliteration to reduce stroke in cardiac surgical patients with atrial fibrillation. *Ann. Thorac. Surg.* 61:755–759, 1996. doi:10.1016/0003-4975(95)00887-X.

[5]Brambatti, M., S. J. Connolly, M. R. Gold, C. A. Morillo, A. Capucci, C. Muto, C. P. Lau, I. C. Van Gelder, S. H. Hohnloser, M. Carlson, E. Fain, J. Nakamya, G. H. Mairesse, M. Halytska, W. Q. Deng, C. W. Israel, and J. S. Healey. Temporal relationship between subclinical atrial fibrillation and embolic events. *Circulation* 129:2094–2099, 2014. doi:10.1161/CIRCULATIONAHA.113.007825.

[6]Chnafa, C., S. Mendez, and F. Nicoud. Image-based large-eddy simulation in a realistic left heart. *Comput. Fluids* 94:173–187, 2014. doi:10.1016/j.compfluid.2014.01.030.

[7]Daccarett, M., T. J. Badger, N. Akoum, N. S. Burgon, C. Mahnkopf, G. Vergara, E. Kholmovski, C. J. McGann, D. Parker, J. Brachmann, R. S. MacLeod, and N. F. Marrouche. Association of left atrial fibrosis detected by delayed-enhancement magnetic resonance imaging and the risk of stroke in patients with atrial fibrillation. *J. Am. Coll. Cardiol.* 57:831, 2011. doi:10.1016/j.jacc.2010.09.049.

[8]Daoud, E. G., T. V. Glotzer, D. G. Wyse, M. D. Ezekowitz, C. Hilker, J. Koehler, P. D. Ziegler, and T. Investigators. Temporal relationship of atrial tachyarrhythmias, cerebrovascular events, and systemic emboli based on stored device data: a subgroup analysis of TRENDS. *Heart Rhythm* 8:1416–1423, 2011. doi:10.1016/j.hrthm.2011.04.022.

[9]Di Biase, L., P. Santangeli, M. Anselmino, P. Mohanty, I. Salvetti, S. Gili, R. Horton, J. E. Sanchez, R. Bai, S. Mohanty, A. Pump, M. Cereceda Brantes, G. J. Gallinghouse, J. D. Burkhardt, M. Cereceda Brantes, F. Cesarani, M. Scaglione, A. Natale, and F. Gaita. Does the left atrial appendage morphology correlate with the risk of stroke in patients with atrial fibrillation? Results from a multicenter study. *J. Am. Coll. Cardiol.* 60:531–538, 2012. doi:10.1016/j.jacc.2012.04.032.

[10]Fatema, K., K. R. Bailey, G. W. Petty, I. Meissner, M. Osranek, A. A. Alsaileek, B. K. Khandheria, T. S. Tsang, and J. B. Seward. Increased left atrial volume index: potent biomarker for first-ever ischemic stroke. *Mayo Clin. Proc.* 83:1107–1115, 2008. doi:10.4065/83.10.1107.

[11]Fyrenius, A., L. Wigström, T. Ebbers, M. Karlsson, J. Engvall, and A. F. Bolger. Three dimensional flow in the human left atrium. *Heart* 86:448–455, 2001. doi:10.1136/heart.86.4.448.

[12]Goubergrits, L., U. Kertzscher, K. Affeld, C. Petz, D. Stalling, and H. C. Hege. Numerical dye washout method as a tool for characterizing the heart valve flow: study of three standard mechanical heart valves. *ASAIO J.* 54:50–57, 2008. doi:10.1097/MAT.0b013e31815c5e38.

[13]Healey, J. S., S. J. Connolly, M. R. Gold, C. W. Israel, I. C. Van Gelder, A. Capucci, C. P. Lau, E. Fain, S. Yang, C. Bailleul, C. A. Morillo, M. Carlson, E. Themeles, E. S. Kaufman, and S. H. Hohnloser. Subclinical atrial fibrillation and the risk of stroke. *N. Engl. J. Med.* 366:120–129, 2012. doi:10.1056/NEJMoa1105575.

[14]Inoue, Y. Y., A. Alissa, I. M. Khurram, K. Fukumoto, M. Habibi, B. A. Venkatesh, S. L. Zimmerman, S. Nazarian, R. D. Berger, H. Calkins, J. A. Lima, and H. Ashikaga. Quantitative tissue-tracking cardiac magnetic resonance (CMR) of left atrial deformation and the risk of stroke in patients with atrial fibrillation. *J. Am. Heart Assoc.* 4:e001844–e001844, 2015. doi:10.1161/JAHA.115.001844.

[15]Khurram, I. M., J. Dewire, M. Mager, F. Maqbool, S. L. Zimmerman, V. Zipunnikov, R. Beinart, J. E. Marine, D. D. Spragg, R. D. Berger, H. Ashikaga, S. Nazarian, and H. Calkins. Relationship between left atrial appendage morphology and stroke in patients with atrial fibrillation. *Heart*

Rhythm 10:1843–1849, 2013. doi:10.1016/j.hrthm.2013.09.065.

[16]Kim, T., A. Y. Cheer, and H. A. Dwyer. A simulated dye method for flow visualization with a computational model for blood flow. *J. Biomech*. 37:1125–1136, 2004. doi:10.1016/j.jbiomech.2003.12.028.

[17]Kimura, T., S. Takatsuki, K. Inagawa, Y. Katsumata, T. Nishiyama, N. Nishiyama, K. Fukumoto, Y. Aizawa, Y. Tanimoto, K. Tanimoto, M. Jinzaki, and K. Fukuda. Anatomical characteristics of the left atrial appendage in cardiogenic stroke with low CHADS2 scores. *Heart Rhythm* 10:921–925, 2013. doi:10.1016/j.hrthm.2013.01.036.

[18]Kizer, J. R., J. N. Bella, V. Palmieri, J. E. Liu, L. G. Best, E. T. Lee, M. J. Roman, and R. B. Devereux. Left atrial diameter as an independent predictor of first clinical cardiovascular events in middle-aged and elderly adults: the Strong Heart Study (SHS). *Am. Heart J*. 151:412–418, 2006. doi:10.1016/j.ahj.2005.04.031.

[19]Koizumi, R., K. Funamoto, T. Hayase, Y. Kanke, M. Shibata, Y. Shiraishi, and T. Yambe. Numerical analysis of hemodynamic changes in the left atrium due to atrial fibrillation. *J. Biomech*. 48:472–478, 2015. doi:10.1016/j.jbiomech.2014.12.025.

[20]Ku, D. N. Blood flow in arteries. *Annu. Rev. Fluid Mech*. 29:399–434, 1997. doi:10.1146/annurev.fluid.29.1.399.

[21]Miller, J. M., C. E. Rochitte, M. Dewey, A. Arbab-Zadeh, H. Niinuma, I. Gottlieb, N. Paul, M. E. Clouse, E. P. Shapiro, J. Hoe, A. C. Lardo, D. E. Bush, A. de Roos, C. Cox, J. Brinker, and J. A. C. Lima. Diagnostic performance of coronary angiography by 64-row CT. *N. Engl. J. Med*. 359:2324–2336, 2008. doi:10.1056/NEJMoa0806576.

[22]Morales, H., I. Larrabide, A. Geers, L. San Roman, J. Blasco, J. Macho, and A. Frangi. A virtual coiling technique for image-based aneurysm models by dynamic path planning. *IEEE Trans. Med. Imaging* 1–11, 2012. doi:10.1109/TMI.2012.2219626.

[23]Ozer, N., L. Tokgozoglu, K. Ovunc, G. Kabakci, S. Aksoyek, K. Aytemir, and S. Kes. Left atrial appendage function in patients with cardioembolic stroke in sinus rhythm and atrial fibrillation. *J. Am. Soc. Echocardiogr*. 13:661–665, 2000. doi:10.1067/mje.2000.105629.

[24]Piccini, J. P., and J. P. Daubert. Atrial fibrillation and stroke: it's not necessarily all about the rhythm. *Heart Rhythm* 8:1424–1425, 2011. doi:10.1016/j.hrthm.2011.05.005.

[25]Pourmorteza, A., K. H. Schuleri, D. A. Herzka, A. C. Lardo, and E. R. McVeigh. A new method for cardiac computed tomography regional function assessment: Stretch quantifier for endocardial engraved zones (SQUEEZ). *Circ. cardiovasc. Imaging* 5:243–250, 2012. doi:10.1161/CIRCIMAGING.111.970061.

[26]Russo, C., Z. Jin, R. Liu, S. Iwata, A. Tugcu, M. Yoshita, S. Homma, M. S. V. Elkind, T. Rundek, C. Decarli, B. Wright, R. L. Sacco, and M. R. Di Tullio. LA volumes and reservoir function are associated with subclinical cerebrovascular disease: The CABL (Cardiovascular Abnormalities and Brain Lesions) study. *JACC. Cardiovasc. Imaging* 6:313–324, 2013. doi:10.1016/j.jcmg.2012.10.019.

[27]Seo, J. H., and R. Mittal. Effect of diastolic flow patterns on the function of the left ventricle. *Phys. Fluids* 25:110801, 2013. doi:10.1063/1.4819067.

[28]Seo, J. H., V. Vedula, T. Abraham, A. C. Lardo, F. Dawoud, H. Luo, and R. Mittal. Effect of the mitral valve on diastolic flow patterns. *Phys. Fluids* 26:121901, 2014. doi:10.1063/1.4904094.

[29]Smiseth, O. A., C. R. Thompson, K. Lohavanichbutr, H. Ling, J. G. Abel, R. T. Miyagishima, S. V. Lichtenstein, and J. Bowering. The pulmonary venous systolic flow pulse–its origin and relationship to left atrial pressure. *J. Am. Coll. Cardiol*. 34:802–809, 1999. doi:10.1016/S0735-1097(99)00300-9.

[30]Tsang, T. S. M., W. P. Abhayaratna, M. E. Barnes, Y. Miyasaka, B. J. Gersh, K. R. Bailey, S. S. Cha, and J. B. Seward. Prediction of cardiovascular outcomes with left atrial size: Is volume superior to area or diameter? *J. Am. Coll. Cardiol*. 47:1018–1023, 2006. doi:10.1016/j.jacc.2005.08.077.

[31]Vedula, V., R. George, L. Younes, and R. Mittal. Hemodynamics in the left atrium and its effect on ventricular flow patterns. *J. Biomech. Eng*. 2015. doi:10.1115/1.4031487.

[32]Wolf, P. A., R. D. Abbott, and W. B. Kannel. Atrial fibrillation as an independent risk factor for stroke: the Framingham study. *Stroke* 22:983–988, 1991. doi:10.1161/01.STR.22.8.983.

[33]Wong, J. M., C. C. Welles, F. Azarbal, M. A. Whooley, N. B. Schiller, and M. P. Turakhia. Relation of left atrial dysfunction to ischemic stroke in patients with coronary heart disease (from the Heart and Soul Study). *Am. J. Cardiol*. 113:1679–1684, 2014. doi:10.1016/j.amjcard.2014.02.021.

[34]Zhang, L., and M. Gay. Characterizing left atrial appendage functions in sinus rhythm and atrial fibrillation using computational models. *J. Biomech*. 41:2515–2523, 2008. doi:10.1016/j.jbiomech.2008.05.012.